MODIFIED NONCLASSICAL COHERENT STATE: SQUEEZING, ANTIBUNCHING, SUB-POISSONIAN PHOTON STATISTICS, REALIZATION SCHEME WITH THE $\chi^{(2)}$-NONLINEARITY, AND GENERATION OF A MACROSCOPIC ENTANGLED STATE

S. A. Podoshvedov [*]

School of Computational Sciences, Korea Institute for Advanced Study
130-722, Seoul, Republic of South Korea

The nonlinear $\chi^{(2)}$ Mach–Zehnder interferometer is proposed as a device for conditional generation of a modified coherent nonclassical state. We show that the generated macroscopic state exhibits nonclassical effects, such as squeezing, photon antibunching, and sub-Poissonian statistics. The modified coherent state generates a macroscopic entangled state. The scheme works without the photon number resolving detection but requires high-efficiency photodetectors. We explain a mechanism of generation of the modified coherent nonclassical state.

PACS: 42.50.Dv

1. INTRODUCTION

The Schrödinger cat paradox [1] is a famous illustration of entanglement between microscopic (a radioactive atom) and macroscopic (a cat) systems; cat-type states given by quantum superpositions of macroscopic systems are a direct consequence of this effect. Cat states play an essential role in both understanding of the unusual behavior of macroscopic entangled systems and quantum information processing [2]. As a result, the problem of generation of cat states attracts considerable interest [3–10]. Schrödinger-cat-type states [3–7] have been realized in quantized cavity fields [8], ion traps [9], and Rydberg atoms [10]. Protocols for teleporting cat states in free propagating fields have been studied in [11]. So far, a number of other possible applications including quantum computation [12], quantum nonlocality test [13], entanglement purification [14], error correction [15], and quantum metrology [16] have been extensively studied with entangled coherent states.

When we talk about a cat state, we usually mean a superposition state of two coherent states with equal amplitudes but opposite phases. The Kerr nonlinearity

[*]E-mail: sap@kias.re.kr

or the $\chi^{(3)}$-nonlinearity is considered to be the resource for the generation of a coherent superposition [3]. But there are significant difficulties in practically realizing the coherent state superposition with a large amplitude due to small values of the $\chi^{(3)}$-nonlinearity of the currently available nonlinear media [7]. The most attractive schemes for generation of the free propagating coherent state superposition were developed in [17]. In essence, these schemes are amplification schemes for the superposition of small-amplitude coherent states obtained from the weak Kerr nonlinearity. These schemes use the squeezed single-photon and simple all-optical operations to amplify the amplitude of the free propagating coherent state superposition with high fidelity. The scheme in [17] has been extensively analyzed in [18] as regards considerably reducing the required nonlinear effect by using simple and efficient optical elements.

Recently, we have proposed using the $\chi^{(2)}$-nonlinearity (with $\chi^{(2)} \gg \chi^{(3)}$) for producing macroscopic entangled states [19, 20] that consist of coherent and modified coherent states. In this paper, we propose a scheme of a nonlinear $\chi^{(2)}$ Mach–Zehnder interferometer to conditionally produce this pure modified coherent state, which we call the $|\beta\rangle$ state. In a certain sense, the proposed scheme of the non-

linear $\chi^{(2)}$ Mach−Zehnder interferometer resembles the nonlinear Mach−Zehnder interferometer with an internal Kerr medium in one arm [6], but the outputs of these devices are different. We present a physical explanation of the generation of the $|\beta\rangle$ state. We show that the $|\beta\rangle$ state has nonclassical properties such as squeezing, photon antibunching, and sub-Poissonian statistics. We show how the $|\beta\rangle$ state can be converted to a macroscopic entangled state. The amount of entanglement stored in the entangled state depends on the amplitude of the coherent state that pumps the nonlinear $\chi^{(2)}$ Mach−Zehnder interferometer. We show that the nonlinear $\chi^{(2)}$ Mach−Zehnder interferometer works without special detectors discriminating between one- and multi-photon number states [21]. We analyze the requirements that must be imposed on detection efficiency of the $\chi^{(2)}$ Mach−Zehnder interferometer to successfully generate the $|\beta\rangle$ state.

2. A NONLINEAR $\chi^{(2)}$ MACH−ZEHNDER INTERFEROMETER

The scheme in Fig. 1 essentially involves a simple Mach−Zehnder interferometer with two input and two output ports. A nonlinear $\chi^{(2)}$ crystal is placed within one arm of the interferometer. We call such an interferometer with an internal second-order nonlinearity the nonlinear $\chi^{(2)}$ Mach−Zehnder interferometer. The nonlinear $\chi^{(2)}$ Mach−Zehnder interferometer is turned on if we direct a powerful beam in the coherent state $|\sqrt{2}\,\alpha\rangle_p$ (the amplitude of the coherent state α is supposed to be real) to the spontaneous parametric down-converter with type-I phase matching (SPDCI).

Before we turn on the powerful mode for the SPDCI, the nonlinear $\chi^{(2)}$ Mach−Zehnder interferometer is a simple Mach−Zehnder interferometer with equal optical paths. Below, we deal with only beam splitters of the Mach−Zehnder interferometer with the Hadamard unitary operation

$$H = \frac{(|0\rangle + |1\rangle)\,\langle 0| + (|0\rangle - |1\rangle)\,\langle 1|}{\sqrt{2}}.$$

If we place two photodetectors behind the routes of the Mach−Zehnder interferometer, then there is 100 % probability that the photon reaches the detector D_1 and 0 % probability that it reaches another detector D_3 in Fig. 1. It is therefore perfectly legitimate to say that the photon takes both the transmitted and the reflected paths between the two beam splitters or, in other words, that the photon is in the coherent superposition
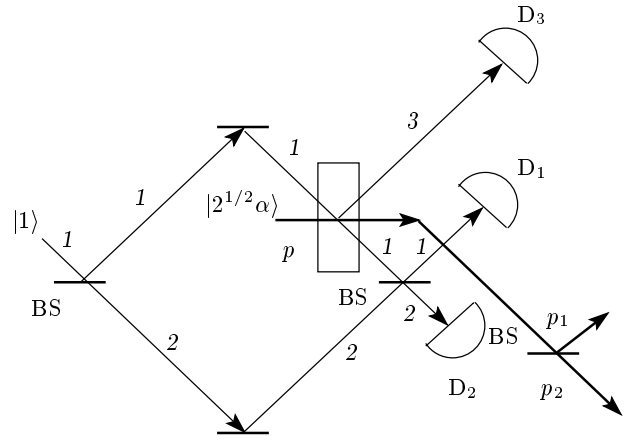

Fig. 1. Experimental arrangement of the nonlinear $\chi^{(2)}$ Mach−Zehnder interferometer. The scheme involves a source of single photons and a Mach−Zehnder interferometer with equal optical paths. Parametric down-converters with type-I phase matching are inserted into one of the routes of the Mach−Zehnder interferometer. A photon that enters the interferometer always strikes detector D_1 if the SPDCI is turned off. By turning SPDCI on, we redirect the photon from detector D_1 to detector D_3 because the single-particle interference is modified due to the interaction of the photons with the $\chi^{(2)}$-nonlinearity. The photon ending up in detector D_2 leads to conditional generation of the macroscopic nonclassical state $|\beta\rangle$. D_1, D_2, and D_3 are registering detectors used in the auxiliary modes. BS is the notation for a beam splitter with the Hadamard unitary operation

$$\frac{|10\rangle_{12} + |01\rangle_{12}}{\sqrt{2}}$$

carrying which-path information.

We next turn on a powerful field in the pumping mode of the SPDCI, giving the total input state

$$|\Psi_{IN}\rangle = \frac{1}{\sqrt{2}}\left(|100\rangle + |010\rangle \right)_{123} |\sqrt{2}\,\alpha\rangle_p \qquad (1)$$

within the nonlinear $\chi^{(2)}$ Mach−Zehnder interferometer, with the auxiliary three generated modes of the SPDCI taken into account. Henceforth, the subscripts of the states indicate the optical modes of photons [22].

For simplicity, we assume that the dynamical description of the SPDCI involves three modes with the corresponding annihilation operators $\hat{a}_1$, $\hat{a}_2$, and $\hat{a}_p$ and that the Hamiltonian [19, 20]

$$\hat{H} = \frac{i\hbar r}{2}\left(\hat{a}_1^+ \hat{a}_3^+ \hat{a}_p - \hat{a}_p^+ \hat{a}_3 \hat{a}_1 \right) \qquad (2)$$

is used. The coupling coefficient r in (2) is related to the nonlinear second-order susceptibility tensor

$\chi^{(2)}$ [19, 20]. The effect of the $\chi^{(2)}$-nonlinearity of the medium has been studied in detail in [19, 20]. Before we proceed with the analysis, we recall the main results in [19, 20]. The input state $|100\rangle_{123}|\alpha\rangle_p$ is transformed into the output state [20]

$$|\Psi_{out}^{(1)}\rangle = \sum_{n=0}^{\infty} |n+1\rangle_1 |1\rangle_2 |n\rangle_3 |\Phi_n^{(1)}\rangle_p, \qquad (3a)$$

with the output states in the pumping modes given by [20]

$$|\Phi_n^{(1)}\rangle_p = \exp(-\alpha^2) \times$$
$$\times \sum_{l=0}^{\infty} \frac{(\sqrt{2}\,\alpha)^{l+n}}{\sqrt{(l+n)!}} f_{(2(l+n)+1),n+1}^{(1)}(\eta)|l\rangle_p. \quad (3b)$$

By analogy with Eqs. (3a) and (3b), if the input state is prepared in the state $|010\rangle_{123}|\alpha\rangle_p$, then its output becomes [19]

$$|\Psi_{out}^{(0)}\rangle = \sum_{n=0}^{\infty} |n\rangle_1 |1\rangle_2 |n\rangle_3 |\Phi_n^{(0)}\rangle_p, \qquad (4a)$$

where the wave functions $|\Phi_n^{(0)}\rangle_p$ are

$$|\Phi_n^{(0)}\rangle_p = \exp(-\alpha^2) \times$$
$$\times \sum_{l=0}^{\infty} \frac{(\sqrt{2}\,\alpha)^{l+n}}{\sqrt{(l+n)!}} f_{2(l+n),n+1}^{(0)}(\eta)|l\rangle_p. \quad (4b)$$

The notation in Eqs. (3a)–(4b) is the same as in [19, 20]. We note that the wave amplitudes $f_{(2(l+n)+1),n+1}^{(1)}$ and $f_{2(l+n),n+1}^{(0)}$ in Eqs. (3b) and (4b) satisfy the sets of linear differential equations presented in [19, 20].

By virtue of the linearity of quantum mechanics, the output of Hamiltonian (2) with input condition (1) can be expressed as

$$|\Psi_{out}\rangle = \frac{1}{\sqrt{2}} \left\{ |\Psi_{out}^{(0)}\rangle + |\Psi_{out}^{(1)}\rangle \right\}. \qquad (5)$$

The overall output $|\Psi_{out}\rangle$ can be rewritten explicitly as

$$|\Psi_{out}\rangle = \frac{1}{\sqrt{2}} \left\{ |100\rangle_{123}|\Phi_0^{(1)}\rangle_p + |010\rangle_{123}|\Phi_0^{(0)}\rangle_p + \right.$$
$$\left. + |111\rangle_{123}|\Phi_1^{(0)}\rangle_p + |201\rangle_{123}|\Phi_1^{(1)}\rangle_p + \ldots \right\}. \quad (6)$$

Using the asymptotic decomposition for the wave amplitudes $f_{2l,k}^{(0)}(\eta)$ and $f_{2l+1,k}^{(1)}(\eta)$ in the leading order with respect to the small parameter $\eta \ll 1$ [19, 20] that characterizes the strength of the SPDCI and is directly pro-

portional to the component of the tensor of the second-order susceptibility,

$$f_{2l,1}^{(0)}(\eta) = 1 - \frac{l\eta^2}{2}, \quad f_{2l+1,1}^{(1)}(\eta) = 1 - l\eta^2,$$
$$f_{2l,2}^{(00)}(\eta) = \eta\sqrt{l}\left(1 - \frac{\eta^2(5l-4)}{6}\right), \qquad (7)$$
$$f_{2l+3,2}^{(00)}(\eta) = \eta\sqrt{2(l+1)}\left(1 - \frac{\eta^2(4l+1)}{3}\right),$$

we find the nonnormalized wave functions in the pumping mode as

$$|\Phi_0^{(0)}\rangle_p = |\sqrt{2}\,\alpha\rangle_p - \frac{\sqrt{2}\,\alpha\eta^2\sqrt{1+2\alpha^2}}{2}|\sqrt{2}\,\beta\rangle_p, \quad (8a)$$

$$|\Phi_0^{(1)}\rangle_p = |\sqrt{2}\,\alpha\rangle_p - \sqrt{2}\,\alpha\eta^2\sqrt{1+2\alpha^2}\,|\sqrt{2}\,\beta\rangle_p, \quad (8b)$$

$$|\Phi_1^{(0)}\rangle_p = \sqrt{2}\,\alpha\eta\left(\left(1 - \frac{\eta^2}{6}\right)|\sqrt{2}\,\alpha\rangle_p - \right.$$
$$\left. - \frac{5\sqrt{2}\,\alpha\eta^2\sqrt{1+2\alpha^2}}{6}|\sqrt{2}\,\beta\rangle_p\right), \quad (8c)$$

$$|\Phi_1^{(1)}\rangle_p = \sqrt{2}\,\alpha\eta\left(\left(1 - \frac{\eta^2}{3}\right)|\sqrt{2}\,\alpha\rangle_p - \right.$$
$$\left. - \frac{4\sqrt{2}\,\alpha\eta^2\sqrt{1+2\alpha^2}}{3}|\sqrt{2}\,\beta\rangle_p\right), \quad (8d)$$

where the normalized macroscopic state $|\beta\rangle$ is defined by

$$|\beta\rangle = \frac{\exp\left(-\dfrac{\alpha^2}{2}\right)}{\alpha\sqrt{1+\alpha^2}} \sum_{l=1}^{\infty} \frac{\alpha^l l}{\sqrt{l!}}|l\rangle. \qquad (9)$$

To finish performance of the nonlinear $\chi^{(2)}$ Mach–Zehnder interferometer in Fig. 1, we erase the which-way information that resides in modes 1 and 2. Two single-photon detectors D_1 and D_2 are attached to the outputs of the output beam splitter of the nonlinear $\chi^{(2)}$ Mach–Zehnder interferometer. The beam splitter with the unitary Hadamard transformation produces the transformations

$$\hat{U}_H |100\rangle_{123} = \frac{1}{\sqrt{2}}\left\{|100\rangle + |010\rangle\right\}_{123},$$
$$\hat{U}_H |010\rangle_{123} = \frac{1}{\sqrt{2}}\left\{|100\rangle - |010\rangle\right\}_{123},$$
$$\hat{U}_H |201\rangle_{123} = \frac{1}{2}\left\{|201\rangle + \sqrt{2}|111\rangle + |021\rangle\right\}_{123}, \quad (10)$$
$$\hat{U}_H |111\rangle_{123} \to \frac{1}{\sqrt{2}}\left\{|201\rangle - |021\rangle\right\}_{123}.$$

Then, after superimposing modes 1 and 2 on the beam splitter, the state $|\Psi_{out}\rangle$ (Eq. (6)) becomes

$$|\Psi_{out}\rangle = \frac{1}{2}\left\{ p_{100}|100\rangle_{123}|\xi\rangle_p - p_{010}|010\rangle_{123}|\sqrt{2}\,\beta\rangle_p + \right.$$
$$+ p_{201}|201\rangle_{123}|\tau_1\rangle_p - p_{021}|021\rangle_{123}|\tau_2\rangle_p +$$
$$\left. + p_{111}|111\rangle_{123}|\tau_3\rangle_p + \dots \right\}, \quad (11)$$

where we introduce the normalized states

$$|\xi\rangle_p = \frac{|\sqrt{2}\,\alpha\rangle_p - \dfrac{3\sqrt{2}\,\alpha\eta^2\sqrt{1+2\alpha^2}\,|\sqrt{2}\,\beta\rangle_p}{4}}{\sqrt{1-3\alpha^2\eta^2 + \dfrac{9\alpha^2\eta^4(1+2\alpha^2)}{8}}}, \quad (12a)$$

$$|\tau_1\rangle_p =$$
$$= \frac{|\sqrt{2}\,\alpha\rangle_p - \dfrac{13\sqrt{2}\,\alpha\eta^2\sqrt{1+2\alpha^2}\,|\sqrt{2}\,\beta\rangle_p}{12(1-\eta^2/4)}}{\sqrt{1-\dfrac{13\alpha^2\eta^2}{3(1-\eta^2/4)} + \left(\dfrac{13\sqrt{2}\,\alpha\eta^2\sqrt{1+2\alpha^2}}{12(1-\eta^2/4)}\right)^2}}, \quad (12b)$$

$$|\tau_2\rangle_p = \frac{|\sqrt{2}\,\alpha\rangle_p + 3\sqrt{2}\,\alpha\sqrt{1+2\alpha^2}\,|\sqrt{2}\,\beta\rangle_p}{\sqrt{1+12\alpha^2+18\alpha^2(1+2\alpha^2)}}, \quad (12c)$$

$$|\tau_3\rangle_p =$$
$$= \frac{|\sqrt{2}\,\alpha\rangle_p - \dfrac{4\sqrt{2}\,\alpha\eta^2\sqrt{1+2\alpha^2}\,|\sqrt{2}\,\beta\rangle_p}{3(1-\eta^2/3)}}{\sqrt{1-\dfrac{16\alpha^2\eta^2}{3(1-\eta^2/3)} + \left(\dfrac{4\sqrt{2}\alpha\eta^2\sqrt{1+2\alpha^2}}{3(1-\eta^2/3)}\right)^2}}. \quad (12d)$$

The wave amplitudes f_{ijk} in Eq. (11), where the subscripts indicate the number of the incoming down-converted photons in modes 1, 2, and 3, are given by

$$p_{100} = 2\sqrt{1 - 3^2\eta^2 + \frac{9\alpha^2\eta^4(1+2\alpha^2)}{8}}, \quad (13a)$$

$$p_{010} = -\frac{\alpha\eta^2\sqrt{1+2\alpha^2}}{\sqrt{2}}, \quad (13b)$$

$$p_{201} = 2\sqrt{2}\,\alpha\eta\left(1 - \frac{\eta^2}{4}\right) \times$$
$$\times \sqrt{1 - \frac{13\alpha^2\eta^2}{3(1-\eta^2/4)} + \left(\frac{13\sqrt{2}\,\alpha\eta^2\sqrt{1+2\alpha^2}}{12(1-\eta^2/4)}\right)^2}, \quad (13c)$$

$$p_{021} = -\frac{\sqrt{2}\,\alpha\eta^3}{6}\sqrt{1+12\alpha^2+18\alpha^2(1+2\alpha^2)}, \quad (13d)$$

$$p_{111} = 2\alpha\eta\left(1 - \frac{\eta^2}{3}\right) \times$$
$$\times \sqrt{1 - \frac{1-16\alpha^2\eta^2}{3(1-\eta^2/3)} + \left(\frac{4\sqrt{2}\,\alpha\eta^2\sqrt{1+2\alpha^2}}{3(1-\eta^2/3)}\right)^2}. \quad (13e)$$

Depending on the result of the single-photon detection, the state $|\Psi_{out}\rangle$ in Eq. (11) becomes either $|\xi\rangle_p$ in Eq. (12a) if detector D_1 fires or $|\sqrt{2}\,\beta\rangle_p$ in Eq. (9) if D_2 does. If the pair of detectors D_1 and D_3, D_2, and D_3 or all three detectors D_1 and D_2, D_3 register three photons, then the total state $|\Psi_{out}\rangle$ in Eq. (11) is projected onto one of the states $|\tau_i\rangle_p$, $i = 1, 2, 3$ (Eqs. (12b)–(12d)). We are interested in generation of the $|\sqrt{2}\,\beta\rangle_p$ state. The overall success probability of the conditional production of the state in the scheme in Fig. 1 is equal to

$$\frac{\alpha^2\eta^4(1+2\alpha^2)}{2}.$$

As noted above, the photon always strikes the detector D_1 and never detector D_2 in the arrangement of the Mach−Zehnder interferometer used in Fig. 1 without pumping of the SPDCI due to single-particle interference. But if we introduce a certain fixed-time delay for the photon to reach the output beam splitter of the Mach−Zehnder interferometer, it may happen that a photon certainly emerges at detector D_2 instead of D_1. Such a time delay can be organized by inserting a glass with some thickness. If we insert the glass in one of the arms of the Mach−Zehnder interferometer with an arbitrary thickness, we observe that the photon may strike both detectors D_1 and D_2 with some success probabilities. We now use a powerful field for the SPDCI in a coherent state as the "time delay" for a single photon. Although the nonlinear effect of the interaction of light fields on the $\chi^{(2)}$-nonlinearity is typically too weak, it can nevertheless play the role of a glass plate. Superimposing the modes of the Mach−Zehnder interferometer on the output beam splitter leads to interferention of the output states in the pumping modes. If a single photon is detected at detector D_1, the superpositions in (8a) and (8b) are superimposed on each other with equal phases and result is the state (12a) in which the contribution of the coherent states prevail over that of the $|\beta\rangle$ state. If the detector D_2 registers a single photon, but the other detectors do not, then superpositions (8a) and (8b) are summed with opposite phases, which leads to the disappearance of the coherent state at the output. Thus, the nonlinear $\chi^{(2)}$ Mach−Zehnder interferometer in Fig. 1 allows the photon to take the route of detector D_1 with almost unit success probability (Eq. (13a)) and the rare chance (Eq. (13b)) for the same photon to come out from the forbidden route of the Mach−Zehnder interferometer leads to the generation of the $|\beta\rangle$ state.

3. NONCLASSICAL PROPERTIES OF THE $|\beta\rangle$ STATE

We now study nonclassical properties of the generated single-mode macroscopic state $|\beta\rangle$ with an arbitrary amplitude of the parameter α (Eq. (9)). There are three principal phenomena that demonstrate the nonclassical character of light: squeezing, photon antibunching, and sub-Poissonian photon statistics. We start with squeezing. We define one of the two quadrature operators as

$$\hat{X} = \frac{1}{2}\left(\hat{a}\exp(-i\varphi) + \hat{a}^{+}\exp(i\varphi)\right), \qquad (14)$$

where φ is the phase of the local oscillator, assumed to be in a large-amplitude coherent state. Using the definition of the $|\beta\rangle$ state in Eq. (9), we obtain the expectation values of operators as

$$\langle\beta|\hat{a}|\beta\rangle = \alpha\frac{2 + |\alpha|^2}{1 + |\alpha|^2}, \qquad (15a)$$

$$\langle\beta|\hat{a}^2|\beta\rangle = \alpha^2\frac{3 + |\alpha|^2}{1 + |\alpha|^2}, \qquad (15b)$$

$$\langle\beta|\hat{a}^{+}\hat{a}|\beta\rangle = \frac{|\alpha|^4 + 3|\alpha|^2 + 1}{1 + |\alpha|^2}. \qquad (15c)$$

Using Eqs. (15a)–(15c), we can calculate the variance of the measured quadrature operator $\hat{X}$,

$$\hat{V}\left(\hat{X}\right) \equiv \left(\Delta\hat{X}\right)^2 = \langle\hat{X}^2\rangle - \langle\hat{X}\rangle^2,$$

as

$$\hat{V}_{|\beta\rangle}\left(\hat{X}\right) = \frac{|\alpha|^4 + 4|\alpha|^2\left(1 - \cos^2(\varphi_\alpha - \varphi)\right) + 3}{4\left(1 + |\alpha|^2\right)^2}, \quad (16a)$$

where φ_α is the phase of α (i.e., $\alpha = |\alpha|\exp(i\varphi_\alpha)$). The degree of single-mode squeezing is assessed by the scaled quantity S, which takes the minimum value at $\varphi_\alpha - \varphi = 0, \pm\pi$:

$$S\left(\hat{X}\right) \equiv S(x) = \frac{\hat{V}_{|\beta\rangle}\left(\hat{X}\right)}{\hat{V}_{|\alpha\rangle}\left(\hat{X}\right)} =$$

$$= \frac{3 + |\alpha|^4}{(1 + |\alpha|^2)^2} = 1 - 2\frac{x - 1}{(x + 1)^2}, \quad (16b)$$

where $\hat{V}_{|\alpha\rangle}\left(\hat{X}\right) = 0.25$ is the variance for the coherent $|\alpha\rangle$ state and $x = |\alpha|^2$. In Fig. 2a, we draw the scaled degree $S(x)$ as a function of $x = |\alpha|^2$. We see from Fig. 2a that the degree of squeezing $S(x)$ is greater than one (to be more precise, we have to talk about de-squeezing in the range) when $0 \le x \le 1$. As x becomes

greater than 1, squeezing appears ($S(x) < 1$), asymptotically approaching unity ($S(x) \to 1$) as $x \to \infty$. There is the value $x = |\alpha|^2 = 3$ at which the degree of squeezing takes the minimum value $S_{min}(x) = 0.75$.

To characterize the statistical properties of the light beam in the modified coherent state $|\beta\rangle$, we introduce the second-order correlation function

$$g^{(2)}(0) = \frac{\langle\hat{a}^{+2}\hat{a}^2\rangle}{\langle\hat{a}^{+}\hat{a}\rangle^2}. \qquad (17a)$$

It is well known that if $g^{(2)}(\tau) > g^{(2)}(0)$, where τ is the time delay of arrival of one photon, with another photon arriving at time t, then there is a tendency for the photons to arrive in pairs. This case is referred to as photon bunching. The opposite situation $g^{(2)}(\tau) < g^{(2)}(0)$ corresponds to the case where close pairs cannot be emitted. It is called the antibunching of photons. We have $g^{(2)}(0) \to 1$ on a sufficiently long time scale, and therefore a field for which $g_2 < 1$ (we now use g_2 instead of $g^{(2)}(0)$) always exhibits antibunching on some time scale. The analytic expression for g_2 for the state $|\beta\rangle$ can be straightforwardly derived from definitions (9) and (17a) as

$$g_2 = \frac{|\alpha|^2\left(|\alpha|^2 + 1\right)\left(|\alpha|^4 + 5|\alpha|^2 + 4\right)}{\left(|\alpha|^4 + 3|\alpha|^2 + 1\right)^2} =$$

$$= \frac{x(x + 1)(x^2 + 5x + 4)}{(x^2 + 3x + 1)^2}. \quad (17b)$$

We plot g_2 versus x in Fig. 2b. This dependence shows that the light generated by the nonlinear $\chi^{(2)}$ Mach–Zehnder interferometer always exhibits photon antibunching ($g_2 < 0$), independent of the value of α.

We next discuss the sub-Poisson statistics in the mode occupied by the state $|\beta\rangle$. The photon-number variance of the mode is given by

$$F = \frac{\langle\Delta\hat{n}^2\rangle}{\langle\hat{n}\rangle} = \frac{|\alpha|^2\left(|\alpha|^4 + 2|\alpha|^2 + 2\right)}{\left(|\alpha|^2 + 1\right)\left(|\alpha|^4 + 3|\alpha|^2 + 1\right)} =$$

$$= \frac{x(x^2 + 2x + 2)}{(x + 1)(x^2 + 3x + 1)}. \quad (18)$$

From Fig. 2b, we see that the $|\beta\rangle$ state exhibits a sub-Poisson statistics $F < 1$ not depending on the value of the parameter α, which can be considered the size of the $|\beta\rangle$ state. Finally, we note the photon number distribution of the $|\beta\rangle$ state

$$P_{|\beta\rangle} = |\langle n|\beta\rangle|^2 = \exp\left(-|\alpha|^2\right)\frac{|\alpha|^{2(n-1)}n^2}{(1 + |\alpha|^2)^2\,n!}. \quad (19)$$
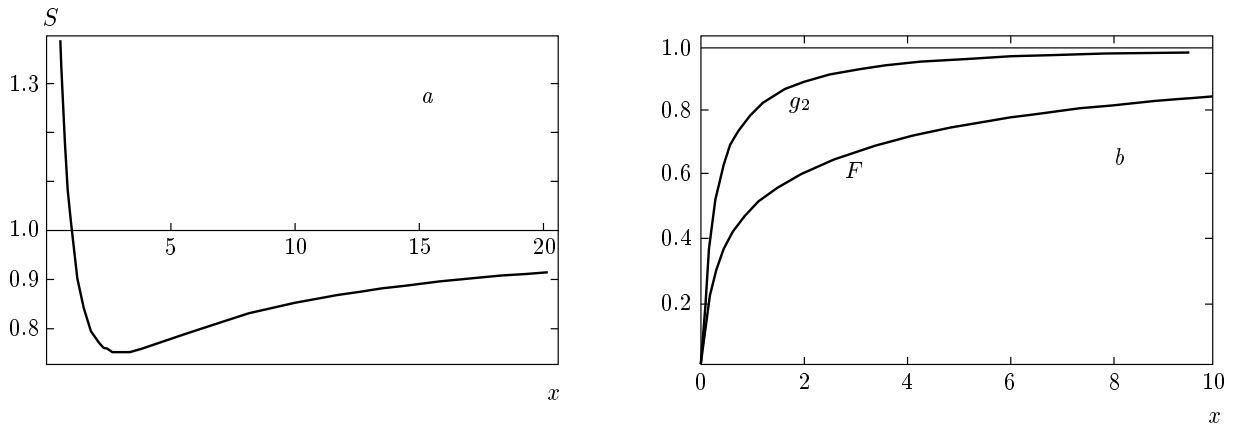
Fig. 2. The dependencies of the squeezing parameter S (a) and the second-order correlation function g_2 and Fano factor F of the $|\beta\rangle$ state on its intensity $x = \alpha^2$ (b)

4. MACROSCOPIC ENTANGLED STATE

At this stage, it is worth considering a possibility of converting the $|\beta\rangle$ state to a macroscopic entangled state. For this, we use the generalized form of the $|\beta\rangle$ state (Eq. (9)) involving the unitary displacement operator $\hat{D}(\alpha) = \exp\left(\alpha\hat{a}^+ - \alpha^*\hat{a}\right)$:

$$|\beta\rangle = \frac{1}{\alpha\sqrt{1+\alpha^2}}\left(\alpha\hat{D}(\alpha)\hat{a}^+|0\rangle + |\alpha|^2|\alpha\rangle\right). \quad (20)$$

We then apply the unitary transformation

$$\hat{U} = \hat{P}_{p_2}(\varphi = \pi/2)\hat{B}(\Theta = -\pi/4)\hat{P}_{p_2}(\varphi = \pi/2),$$

where

$$\hat{P}(\varphi) = \exp\left(-i\varphi\hat{a}^+\hat{a}\right)$$

and

$$\hat{B}(\Theta) = \exp\left(-i\Theta\left(\hat{a}_1^+\hat{a}_2 + \hat{a}_2^+\hat{a}_1\right)\right),$$

to the $|\beta\rangle$ state. Here, p_1 and p_2 are the output modes of the $\hat{U}$ transformation. This unitary transformation is effected by two $\pi/2$ phase shifters and one balanced beam splitter located between these two phase shifters in the p_2 mode. The beam-splitter transformation maps the input $|\beta\rangle$ state into the entangled normalized state

$$\hat{U}|\sqrt{2}\,\beta\rangle_p = |\Delta_+\rangle_{p_1 p_2} = \frac{|\alpha\rangle_{p_1}|\beta\rangle_{p_2} + |\beta\rangle_{p_1}|\alpha\rangle_{p_2}}{\sqrt{2\left(1 + \dfrac{\alpha^2}{1+\alpha^2}\right)}}. \quad (21)$$

This state is analogous to the state studied in [20], but with the plus sign. We estimate the amount of entanglement stored in the states $|\Delta_+\rangle_{p_1 p_2}$ by calculating the concurrence of the state defined in the general form as

$$C\left(|\psi\rangle\right) = \sqrt{2\left(1 - \mathrm{Sp}(\rho_A^2)\right)},$$

where ρ_A is the reduced density matrix of subsystem A [20]. Using the orthonormal basis $\{|0\rangle_{p_i}, |1\rangle_{p_i}\}$,

$$|0\rangle_{p_i} = |\alpha\rangle_{p_i},$$
$$|1\rangle_{p_i} = \frac{|\beta\rangle_{p_i} - a|\alpha\rangle_{p_i}}{\sqrt{1-a^2}}, \quad i = 1, 2, \quad (22a)$$

where

$$a = \langle a|\beta\rangle = \alpha/\sqrt{1+\alpha^2},$$

we rewrite the state $|\Delta_+\rangle_{p_1 p_2}$ Eq. (21) as

$$|\Delta_+\rangle_{p_1 p_2} =$$
$$= \frac{\left(2a|00\rangle + \sqrt{1-a^2}\left(|01\rangle + |10\rangle\right)\right)_{p_1 p_2}}{\sqrt{2(1+a^2)}}. \quad (22b)$$

The concurrence of the state $|\Delta_+\rangle_{p_1 p_2}$ is then given by

$$C\left(|\Delta_+\rangle_{p_1 p_2}\right) = \frac{1-a^2}{1+a^2} = \frac{1}{1+2\alpha^2}. \quad (23)$$

The concurrence of $|\Delta_+\rangle_{p_1 p_2}$ depends on the intensity α^2 of the $|\beta\rangle$ state. It takes the maximum value $C\left(|\Delta_+\rangle_{p_1 p_2}\right) = 1$ at $\alpha = 0$, when the entangled state $|\Delta_+\rangle_{p_1 p_2}$ in Eq. (21) is converted into the one-photon state,

$$|\Delta_+\rangle_{p_1 p_2} \rightarrow \frac{\left(|10\rangle + |01\rangle\right)_{p_1 p_2}}{\sqrt{2}}.$$

If the size α of the entangled state $|\Delta_+\rangle_{p_1 p_2}$ approaches the infinity ($\alpha \rightarrow \infty$), the concurrence goes to zero ($C\left(|\Delta_+\rangle_{p_1 p_2}\right) \rightarrow 0$). This fact is in accordance with Figs. 2a and 2b. As can be seen from Figs. 2a and 2b, the squeezing S and the parameters g_2 and F approach unity ($S, g_2, F \rightarrow 1$) as $\alpha \rightarrow \infty$, which shows that the $|\beta\rangle$ state may become indistinguishable from the usual coherent state $|\alpha\rangle$ for large values of α.

We have shown that generation of the macroscopic $|\beta\rangle$ state by using the nonlinear $\chi^{(2)}$ Mach – Zehnder interferometer can be realized without photon number resolving detection. We now formulate the requirements that must be imposed on the detection efficiency in scheme 1. We assume the detection efficiency of photodetectors in Fig. 1 to be d. Then, the probability for the detector not to register one photon (the failure probability) is $1 - d$. It follows from Eq. (11) that there are two possible failure events, which can be taken for the right outcomes when either the third detector or the first and third detectors simultaneously register any photons, while the second detector registers arrival of some photons. This means that photodetectors are inefficient in practice and may miss some coming photons, and we can therefore sometimes mistake the states $|\tau_2\rangle$ and $|\tau_3\rangle$ (Eqs. (9), (12c), and (12d)) for the $|\sqrt{2}\,\beta\rangle$ state. Therefore, success probabilities for the states $|\sqrt{2}\,\beta\rangle$, $|\tau_2\rangle$, and $|\tau_3\rangle$ in the leading order in η can be estimated as

$$P_{010} \approx \alpha^4\eta^4, \qquad (24\text{a})$$

$$P_{021} \approx 2\alpha^6\eta^6(1-d), \qquad (24\text{b})$$

$$P_{111} \approx 4\alpha^2\eta^2(1-d)^2. \qquad (24\text{c})$$

Detection inefficiency leads to generation of an ensemble of pure states $\{P_{010}, |\beta\rangle; P_{021}, |\tau_2\rangle; P_{11}|\tau_3\rangle\}$ with the respective probabilities P_{010}, P_{021}, and P_{111}. Comparing them, we see that $P_{021} \ll P_{010}, P_{111}$ in the $\alpha\eta \ll 1$ approximation used in practice, which allows ignoring the influence of $|\tau_2\rangle$. Then the density matrix can be approximately written as

$$\rho = \left(1 - \frac{P_{111}}{P_{010}+P_{111}}\right)|\sqrt{2}\,\beta\rangle\langle\sqrt{2}\,\beta| + $$
$$+ \left(1 - \frac{P_{010}}{P_{010}+P_{111}}\right)|\tau_3\rangle\langle\tau_3|. \quad (25)$$

The fidelity

$$F = \langle\sqrt{2}\,\beta|\rho|\sqrt{2}\,\beta\rangle$$

of the scheme in Fig. 1 strongly depends on the efficiency of the detectors and on the value of α. To show this, we take the $|\tau_3\rangle$ state in the form $|\sqrt{2}\,\alpha\rangle_p$ in the $\alpha\eta \ll 1$ approximation. Then the fidelity of the scheme is equal to

$$F = \frac{P_{010} + P_{111}\dfrac{\sqrt{2}\,\alpha}{\sqrt{1+2\alpha^2}}}{P_{010} + P_{111}}. \qquad (26)$$

If the parameter α takes a large value (in limit case $\alpha \to \infty$), then $F \to 1$, which is related to the $|\beta\rangle$ state

becoming indistinguishable from the coherent state $|\alpha\rangle$ as α increases. In the limit of small values of α, in which we are more interested, the fidelity is mainly determined by the ratio of the probability P_{010} to P_{111}. Under this condition, the fidelity between the final state (25) and the ideal output (9) is proportional to

$$1 - \frac{P_{111}}{P_{010} + P_{111}}.$$

Comparing the error probability P_{111} in Eq. (24c) with the success probability P_{010} in Eq. (24a), we see that in order to minimize the influence of the undetected error events ($F \approx 1$) while keeping the value of α small, we need to substantially improve the detection efficiency ($1 - d \ll \alpha\eta$) in the scheme in Fig. 1. If the detection efficiency is comparable to the experimental parameter $\alpha\eta$ ($1 - d \approx \alpha\eta$), we reach half fidelity for the scheme ($F \approx 0.5$). Another way to improve fidelity of the nonlinear $\chi^{(2)}$ Mach – Zehnder interferometer is to use a crystal with a high value of the second-order susceptibility (which in our case means increasing the value of the parameter η), leaving the intensity of the incident light to be low. The influence of the terms with more than three down-converted photons on the fidelity of conditional production of the $|\beta\rangle$ state is negligible.

Examining the final outcome of the studied $\chi^{(2)}$ Mach – Zehnder interferometer may lead to the following question: how can one down-converted photon cause a noticeable variance in the pump field statistics and, as consequence, give a rise to entanglement? We suppose that we take the wave function $|11\rangle_{13}|\alpha\rangle_p$ as an input to Hamiltonian (2) (Fig. 1) and consider the outcome of the second term of Hamiltonian (2) on the input state $|11\rangle_{13}|\alpha\rangle_p$. Then the following chain of transformations holds:

$$\hat{a}_p^+\hat{a}_1\hat{a}_3|11\rangle_{13}|\alpha\rangle_p = $$
$$= \exp(\alpha^2/2)\hat{a}_p^+\hat{a}_1\hat{a}_3|11\rangle_{12}\sum_{l=0}^{\infty}\frac{\alpha^l}{\sqrt{l!}}\,|l\rangle_p \to$$
$$\to \exp(\alpha^2/2)|00\rangle_{13}\sum_{l=0}^{\infty}\frac{\alpha^l\sqrt{l+1}}{\sqrt{l!}}\,|l+1\rangle_p\,(m = l+1) \to$$
$$\to \frac{\exp(\alpha^2/2)}{\alpha}|00\rangle_{13}\sum_{m=1}^{\infty}\frac{\alpha^m m}{\sqrt{m!}}\,|m\rangle_p = $$
$$= \sqrt{1+\alpha^2}\,|00\rangle_{13}|\beta\rangle_p. \quad (27)$$

As can be seen from (27), the spontaneous up-conversion leads to to the $|\beta\rangle$ state when two down-converted photons are annihilated. The success probability of the up-conversion is comparable to the success probability

of the generation of a pair of down-converted photons ($\sim \alpha^2 \eta^2$) if we stock two input down-converted photons. Where can two down-converted photons arise inside the crystal? Spontaneous down-conversion — the process reverse to spontaneous up-conversion — serves as a resource for the pair of down-converted photons with the success probability also proportional to $\alpha^2 \eta^2$. Therefore, two successive processes of creation and annihilation of two down-converted photons generate the $|\beta\rangle$ state. The total success probability of such a "flip-flop" of a pair of the down-converted photons is of the same order as the success probability of the generation of two pairs of down-converted photons ($\sim \alpha^4 \eta^4$). As shown above, the single photon used in the all-optical scheme of the nonlinear $\chi^{(2)}$ Mach−Zehnder interferometer serves as a trigger to identify the $|\beta\rangle$ state. Indeed, estimations for the input state

$$\hat{a}_1^+ \hat{a}_3^+ \hat{a}_p |10\rangle_{13} |\alpha\rangle_p \to \sqrt{2} |21\rangle_{12} |\alpha\rangle_p$$

(down-conversion),

$$\hat{a}_p^+ \hat{a}_1 \hat{a}_3 \sqrt{2} |21\rangle_{13} |\alpha\rangle_p \to 2\sqrt{1 + \alpha^2} |10\rangle_{13} |\alpha\rangle_p$$

(up-conversion), and chain (27) show that the factors for the $|\beta\rangle$ state are different from each other depending on the presence or absence of a single photon at the input. This difference of the factors is sufficient to obtain a pure nonclassical $|\beta\rangle$ state at the output of the nonlinear $\chi^{(2)}$ Mach−Zehnder interferometer. In the current experiments for generating multiphoton entanglement by using spontaneous parametric down-conversion [23], the photon pair generation rate per pulse ($\alpha^2 \eta^2$ in the units used) is of the order of $5 \cdot 10^{-4}$. Then the generation rate for the expected $|\beta\rangle$ state is of the order 10^{-7}.

We comment on the feasibility of the studied nonlinear $\chi^{(2)}$ Mach−Zehnder interferometer. Our results show that the $|\beta\rangle$ state manifests its nonclassical properties for small values of the parameter α. It is convenient to pass to real values of the field energy within the coherence volume from the dimensionless quantity α^2 that gives the number of photons in the pumping mode. We therefore have

$$n = \alpha^2 = \frac{E_0^2 V_{coh}}{8\pi\hbar\omega_0} = \frac{I\lambda}{hc}\Delta f,$$

where I is the power, λ is the wavelength, and $\Delta f = \Delta\omega/2\pi$ is the spectral bandwidth. Then, for instance, choosing $n = \alpha^2 = 3$ (such that the squeezing degree of the $|\beta\rangle$ state takes the minimum value, see Fig. 2 a), $\Delta f = 10^9$ Hz, and $\lambda = 0.5 \mu$m, we obtain the power of light $1.2 \cdot 10^{-9}$ W. This light flux power is too low to ensure the observation of the $|\beta\rangle$ state with a success probability acceptable in experiment and with a small value of the parameter α. Thus, resonance nonlinear three-photon processes leading to huge values of the $\chi^{(2)}$-nonlinearity must be used to increase the success probability of the $|\beta\rangle$ state generation with a small value of α. As regard a possible strategy to study this problem, we note that if we successfully generated the $|\beta\rangle$ state with a sufficiently large value of α, we can pass the light before detection through a linear absorber with some intensity transmission coefficient. The $|\beta\rangle$ state is a nonclassical state, which is confirmed by the calculation of the squeezing degree and anti-bunching of photocounts, the characteristics being the best known and the simplest criterion of nonclassicality. It is well known that nonclassical light remains nonclassical even after an arbitrarily strong linear absorption [24]: as consequence, nonclassical light gives a rise to entanglement [25]. The study of the nonclassical properties of the $|\beta\rangle$ state, its possible applications, and improvement of the initial scheme in Fig. 1 deserves further investigations.

In conclusion, we have studied a mechanism of generation of a nonclassical $|\beta\rangle$ state using the $\chi^{(2)}$-nonlinearity. For this, an all-optical scheme of the nonlinear $\chi^{(2)}$ Mach−Zehnder interferometer consisting of a source of single photons and a Mach−Zehnder interferometer with a crystal with the second-order susceptibility inserted into one arm is proposed. We identify the $|\beta\rangle$ state through the single photon in the forbidden D_2 route of the Mach−Zehnder interferometer.

REFERENCES

1. E. Schrödinger, Naturwissenschaften **23**, 807 (1935).

2. P. T. Cochrane, G. J. Mulburn, and W. J. Munro, Phys. Rev. Lett. **59**, 2631 (1999).

3. B. Yurke and D. Stoler, Phys. Rev. Lett. **57**, 13 (1986).

4. S. Song, C. M. Caves, and B. Yurke, Phys. Rev. A **41**, 5261 (1990).

5. B. Yurke, W. Schleich, and D. F. Walls, Phys. Rev. A **42**, 1703 (1990).

6. B. C. Sanders, Phys. Rev. A **45**, 6811 (1992); B. C. Sanders and G. J. Milburn, Phys. Rev. A **45**, 1919 (1992); C. C. Gerry, Phys. Rev. A **59**, 4095 (1999).

7. R. W. Boyd, J. Mod. Opt. **46**, 367 (1999).

8. M. Brune, F. Schmidt-Kuler, A. Maali, J. Dreyer, E. Hagley, J. M. Raimond, and S. Haroche, Phys. Rev. Lett. **76**, 1800 (1996).

9. C. Monroe, D. M. Meckhof, B. E. King, and D. J. Wineland, Science **272**, 1131 (1996).

10. N. W. Noel and C. R. Stroud, Jr., Phys. Rev. Lett. **77**, 1913 (1996).

11. X. Wang, Phys. Rev. A **64**, 022302 (2001); S. J. van Enk and O. Hirota, Phys. Rev. A 64, 022313 (2001); S. J. van Enk, Phys. Rev. A **67**, 022318 (2003); H. Jeong, M. S. Kim and J. Lee, Phys. Rev. A **64**, 052308 (2001).

12. H. Jeong and M. S. Kim, Phys. Rev. A **65**, 042305 (2002); T. C. Ralph, A. Gilchrist, G. J. Milburn, W. J. Munro, and S. Glancy, Phys. Rev. A **68**, 042319 (2003).

13. D. Wilson, H. Jeong, and M. S. Kim, J. Mod. Opt. **49**, 851 (2002); H. Jeong, W. Son, M. S. Kim, D. Ahn, and C. Brukner, Phys. Rev. A **67**, 012106 (2003).

14. H. Jeong and M. S. Kim, Quantum Inf. Comput. **2**, 208 (2002); J. Clausen, L. Knöll, and D.-G. Welsch, Phys. Rev. A **66**, 062303 (2002).

15. P. T. Cochrane, G. J. Milburn, and W. J. Munro, Phys. Rev. A **59**, 2631 (1999); S. Glancy, H. Vasconcelos, and T. C. Ralph, E-print archives quant-ph/0311093.

16. T. C. Ralph, Phys. Rev. A **65**, 042313 (2002); W. J. Munro et al., ibid. **66**, 023819 (2002).

17. A. P. Lund, H. Jeong, T. C. Ralph, and M. S. Kim, Phys. Rev. **70**, 020101(R) (2004); H. Jeong, M. S. Kim, T. C. Ralph, and B. S. Ham, Phys. Rev. **70**, 061801(R) (2004).

18. H. Jeong, A. P. Lund, and T. C. Ralph, Phys. Rev. A **72**, 013801 (2005).

19. S. A. Podoshvedov, Zh. Eksp. Teor. Fiz. **129**, 615 (2006); S. A. Podoshvedov, B. A. Nguyen, and J. Kim, J. Modern Optics **53**, 1853 (2006).

20. S. A. Podoshvedov, Phys. Lett. A **357**, 424 (2006); S. A. Podoshvedov and J. Kim, Phys. Rev. A **74**, 033810 (2006).

21. S. Takeuchi, Y. Yamanoto, and H. H. Hogue, Appl. Phys. Lett. **74**, 1063 (1999).

22. M. A. Nielsen and I. L. Chuang, *Quantum Computation and Quantum Information*, Cambridge University Press, Cambridge, United Kingdom (2000).

23. D. Bouwmeester, J.-W. Pan, M. Daniell, H. Weinfurter, and A. Zeilinger, Phys. Rev. Lett. **82**, 1345 (1999); J.-W. Pan et al., Phys. Rev. Lett. **86**, 4435 (2001); J.-W. Pan, D. Bouwmeester, M. Daniell, H. Weinfurter, and A. Zeilinger, Nature **403**, 515 (2000).

24. D. N. Klyshko, Uspekhi Fiz. Nauk **39**, 573 (1996).

25. M. S. Kim, W. Son, V. Busek, and P. L. Knight, Phys. Rev. A **65**, 032323 (2002).